Electric Power Systems Research 248 (2025) 111849

Contents lists available at ScienceDirect

Electric Power Systems Research

journal homepage: www.elsevier.com/locate/epsr

Adaptive mixed time-state dependent distributed event-triggered consensus protocol of a DC microgrids cluster

Zaid Hamid Abdulabbas Al-Tameemi [a,*], Rasool Peykarporsan [a], Tek Tjing Lie [a], Ramon Zamora [a], Frede Blaabjerg [b]

[a] Department of Electrical and Electronic Engineering, Auckland University of Technology, Auckland, 1010, New Zealand
[b] The Faculty of Engineering and Science, Aalborg Universitet, Aalborg, 9220, Denmark

ARTICLE INFO

Keywords:
AMDETC
AFTA
Clustered DCMGs
Current sharing
OPAL-RT
Voltage regulation

ABSTRACT

This paper presents a novel Adaptive Mixed Time-State Dependent Distributed Event-Triggered Consensus Protocol (AMDETC) aimed at achieving less communication requirements among microgrids (MGs) within a cluster. Also, an adaptive fixed-time consensus algorithm (AFTA), enhanced by a saturation function, is incorporated into the secondary control layer to improve currents convergence rates within the cluster. Additionally, the Grey Wolf Optimizer (GWO) technique is utilized to fine-tune the parameters of proportional–integral (PI) controllers at the secondary control level, thus bolstering the cluster's resilience to disturbances. The results demonstrate the proposed control strategy's superiority over current control schemes, particularly in terms of realizing 100% accuracy of triggering instances and achieving rapid currents convergence within 0.02s along with swift voltage recovery under various operational conditions. A simulation involving a cluster of four DC MGs is executed in the MATLAB environment to validate the effectiveness of the proposed control approach against existing control techniques. Moreover, OPAL-RT is employed to validate this technique in a real-life scenario.

1. Introduction

MGs are embedded electrical systems consisting of interconnected distributed generators (DGs), energy storage systems (ESS), and end-use loads [1]. These MGs have been advocated as feasible solutions for creating local grids that use a variety of renewable energy sources (RES) [2] because they allow the integration of RES with ESS to meet energy requirements [3]. Remarkably, DC MGs are proliferating more quickly than their AC counterparts because of their features, such as lower harmonics, absence of frequency synchronization requirements, and more straightforward reactive power regulation in isolated modes [4].

To boost their adaptability and reliability, closely positioned clusters of MGs can be combined [5]. Such combinations provide substantial benefits, including increasing the share of renewable energy while expanding the service area, enhancing system stability in the face of generation and demand fluctuations, and improving the power system's overall efficiency and economic viability. Effective coordination among MGs within a cluster is critical to optimize the use of resources across the cluster. Numerous control strategies have been adopted in the literature to coordinate these MGs in a cluster, including centralized, decentralized, distributed, and hierarchical schemes [6]. The decentralized droop control method has been used to control power distribution and voltage stability, although it can lead to problems, including improper current distribution and voltage fluctuations [7]. The benefit of centralized control is that decisions can be made using information from all MGs, but it also has the drawback of a single point of failure [8]. These problems have been addressed using distributed hierarchical and two-level control approaches [9–11].

To solve the control issues that result from integrating DERs into an MG and coordinating MGs in a cluster, several research have proposed the concept of controlled hierarchy [12–15]. Multiple control levels are used in this approach, which increases the MG's adaptability and effectiveness. This strategy's main advantage is its ability to classify the MG control system into several control layers, offering excellent control reliability and seamless operation in grid-connected modes other than island modes [16].

Although earlier control strategies, including time-triggered consensus, have been successful in achieving precise power distribution and regulation of voltage across clustered MGs, they rely on a specific schedule for updates and information exchange. Because of the frequent updates and the requirement for secure and constant communication

* Corresponding author.
E-mail address: zaid.altameemi@autuni.ac.nz (Z.H.A. Al-Tameemi).

https://doi.org/10.1016/j.epsr.2025.111849
Received 10 December 2024; Received in revised form 23 April 2025; Accepted 15 May 2025

networks, this leads to a major resource consumption [17]. A Distributed Event Control (DETC) method has been proposed as a solution to this problem, which greatly lessens the communication overhead. Different from Distributed Time Control (DTTC), DETC determines when to sample and send data based on a predefined operational condition [18]. When the system error which is the difference between the actual measurements (voltages/currents) and the last triggering instant exceeds a predetermined threshold, the triggering condition is satisfied [19] This activates communication between agents in the system to exchange their data, efficiently linking data sampling, control measures, and system measurements.

This approach has been proposed in AC MGs for frequency and voltage control [20], demand response [21], economic dispatch in smart grids [22], and reactive power control [23]. Additionally, several researchers have investigated controlling DC MGs using a distributed event control approach (DETC). In [24]an event-triggering mechanism with distributed sliding mode control based on leader-follower consensus protocol is presented to regulate voltage in DC MG. The Kalman filter of the event triggering function is used to estimate the voltage of the DC-DC converter and regulate the DC-Link voltage [25]. DETC based on a permissible error threshold is introduced in [26] to achieve average DC bus voltage consensus and accurate current distribution among distributed generators (DGs) in a DC MG. However, the main issue is that the bus voltage must be continuously monitored. In [27], a state-dependent triggering condition threshold addresses average voltage adjustment and proportional distribution of load current in a DC MG. Another state-based event triggering condition is proposed in [20] to tackle the consensus problem in the DC bus voltage along with current sharing of DGs. Also, a periodic event-triggered control approach is considered in [28] to regulate the DC link voltage and share currents among DGs in a MG based on a state-dependent trigger function. An event condition based on a fixed fault threshold is proposed in [29] to regulate voltages and share currents among DGs in a DC MG. An event-triggered multi-layer consensus protocol is introduced at the second and third control layers of a hierarchical control scheme for energy storage systems (ESSs) in DC MGs [30]. The event-triggered consensus algorithm in the second control layer handles current distribution and voltage regulation among ESSs, while the control structure in the third layer regulates global current sharing through pinned ESS updates. A new distributed secondary control approach is presented in [31] to enhance fixed-time convergence, reduce triggering events, and solve power exchange and DC bus voltage adjustment in hybrid ESS DC MG clusters. Furthermore, 5. an adaptive distributed the event-triggered consensus protocol is presented in [32] to manage DC-bus voltage and share load current in DC MG. All of these studies relied on exchanging current and voltage data, adding to communication overhead. Therefore, a new DETC protocol [33–35] addresses this by prioritizing accurate load current sharing and voltage regulation. It exchanges output current information solely between controllers, aided by a voltage observer. Also, mixed time-state dependent distributed event-triggering algorithm is proposed in [36] to enhance current sharing, voltage regulation while reducing the communication burden among MGs in a cluster.

However, these earlier studies encountered several challenges: Most of them relied on state-dependent functions, which could potentially lead to Zeno behavior, indicating the excessive sensitivity of the event trigger consensus algorithm to minor state changes in the system. Additionally, they employed infinite-time consensus at the secondary control level and overlooked the importance of proper PI controller selection, resulting in slower voltage recovery during critical conditions. Moreover, [33–35] primarily focused on addressing DG connection challenges in closely located MGs, neglecting the complexities associated with coordinating MGs across distant clusters. Another notable limitation was the assumption that control coefficients in [33–36] remain fixed across different operational conditions. This assumption is unrealistic because of the unpredictability of fault severity and load changes in real-life scenarios. Once load varies or fault occurs with different severity, the static control coefficients used in these studies impede the adaptability of the cluster, compromising its capability to respond effectively to dynamic operational conditions.

A novel Adaptive mixed time-state dependent distributed event-triggering algorithm based on artificial neural networks (ANN) is introduced in this article to address such challenges in tertiary control layer. The main advantage of this combination is reducing the triggering instances, as illustrated in [37], ensuring that state change triggers events when necessary, which balances responsiveness and communication efficiency. Furthermore, in this study, the control coefficients of this algorithm are consistently updated based on the cluster's conditions, including load changes and faults, which contributes to further reduction in communication among MGs.

Also, In the second control layer of the proposed control scheme, several studies [38–41] has been proposed in the field of time-triggering consensus algorithms to enhance the convergence rates of the cluster currents but the control parameters in these studies are fixed, which not always be able to withstand sudden disturbances in the system, potentially jeopardizing current convergence. Recently, fixed-time consensus algorithm has been incorporated with event-triggered consensus algorithms in the field of DC MGs as shown in [31,38,42]. Authors of [31] present A distributed fixed-time control method implemented to improve current distribution and voltage stability in clusters of DC MGs using hybrid storage systems. The proposed method uses event-trigger communication, fixed-time convergence, and Kalman filtering to reduce communication overhead and ensure reliable performance during time-varying conditions. Furthermore, a distributed event-triggered fixed-time control strategy for the optimal power dispatch and voltage regulation in islanded DC MGs is proposed in [43], obviously addressing input communication delays and limited bandwidth. It requires careful tuning of multiple control parameters, which adds complexity to implementation. However, control coefficient adjustment in [31,42] requires careful tuning, as they directly affect the convergence time, thus making the task of design and implementation more complex. Also, Distributed event-triggered fixed-time control scheme for DC MGs is proposed in [42] to achieve fast voltage recovery and accurate current sharing of DGs. However, the complexities in the tuning of the controller parameters require careful selection to make a trade-off between convergence speed, stability, and communication effectiveness since poor tuning will result in slow responses or oscillatory control signals. Based on a study in [43],a predefined-time-based control scheme of multi-bus DC MGs is proposed in order to control bus voltage, provide accurate current distribution, and reduce transmission losses. This control scheme is guaranteed to achieve control goals at a predefined time through a combined use of a distributed optimization and a predefined-time observer. It should be noted that the control parameters derived by using fixed-time operators in It is obvious that all control coefficients of fixed-time functions adopted in these studies require proper tuning to ensure the accurate convergence rate under critical conditions in a cluster. Therefore, this paper uses a novel adaptive fixed-time consensus algorithm (AFTCA) in [37] in order to overcome the drawback of the algorithms in the above studies, so the robustness of the secondary control layer can be increased in the presence of cluster conditions variations.

Moreover, this study employs the GWO in [2], which is featured by quick convergence, simplicity, ease of implementation [44] and superior performance in unknown, complex search spaces, especially in engineering applications [45] is used to tune the PI controllers of the secondary control layer of the proposed control scheme. The GWO has been demonstrated to outperform the PSO algorithm, bat algorithm, ant-lion algorithm, and gravitational search algorithm [46], further enhancing the cluster's performance under different operating conditions. Therefore, the hybrid GWO-AFTCA is adopted for the first time, to the best our knowledge, substantially enhancing current convergence rates and voltage regulation.

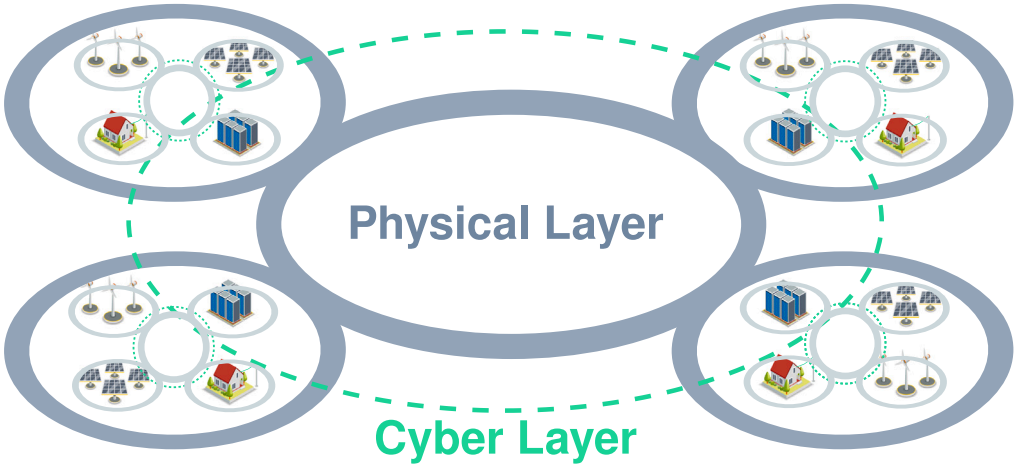

Fig. 1. The configuration of DCMG cluster.

Due to drawbacks of radial configuration, including complex control and management and limited power exchanges because of bus capacity [47], the ring architecture of the four-DC MGs cluster adopted in this study is simulated in the MATLAB environment and then validated in OPAL-RT to assess the effectiveness of the proposed control method. The ring structure is considered an efficient design for multiple MGs Because of its secure fault isolation, high reliability, connection flexibility, increased voltage stability [48], and better economic characteristics while also allowing MGs to operate more autonomously [47].

The key contributions of this paper can be summarized as follows:

1. A novel Adaptive Mixed Time-State Dependent Distributed Event-Triggered Consensus Protocol (AMDETC) is introduced to tackle unnecessary data exchange in a cluster during steady state circumstances.
2. An adaptive Fixed-Time Consensus Algorithm using a saturation function in the secondary control layer is adopted in the secondary control layer to regulate control outputs, avoiding cluster oscillations. This achieves faster current convergence and shorter settling times.
3. GWO is adopted to achieve precise current sharing and DC voltage regulation, even under challenging conditions like load changes, and faults.
4. ANN is used to predict control coefficients in AMDETC based on load changes, and faults which results in 100% triggering instants accuracy.
5. Consideration of operational challenges in coordinating MGs within a cluster is crucial. The proposed control approach effectively minimizes inter-MG communication, thereby reducing the risk of communication delays—an essential concern in MG Clusters (MGCs). It also promotes the cluster's energy-efficient and sustainable operation.

2. Problem formulation

The DC MG cluster, shown in Fig. 1, is organized into two distinct layers: the physical layer and the cyber control layer.

2.1. Physical layer

The MG cluster can be effectively analyzed using graph theory, which poses a perfect framework for representing the physical and cyber aspects of the cluster. A graph consists of two finite sets : vertex $\mathcal{V}$ and edges $\mathcal{E}$ [49]. In the context of a MG cluster, the vertices represent the individual MGs within the cluster, denoted as $\mathcal{V}_e = \{1, 2, \dots, N\}$, where N N is the number of MGs. The edges $\mathcal{E}_e \in \mathcal{V} \times \mathcal{V}$ denote the physical connections between MGs in the cluster, allowing power flow between them. In this study, each MG is equipped with two distributed generation units and DC-DC converters to manage voltage levels and stabilize the current load, as illustrated in Fig. 1. The physical network of the MGs cluster in Fig. 1 is modeled as an indirected weighted graph $\mathcal{G}_e(\mathcal{V}, \mathcal{E}, \mathcal{W})$, where the vertices are the MGs, and the edges represent power lines connecting the MGs in the cluster [33]. The weights ($\mathcal{W}$) on the edges reflect the conductance of these lines, which are assumed to be 1 Ω^{-1}.

To mathematically describe the network structure, The adjacency matrix $\mathcal{A} = [\mathcal{G}_{ij}] \in \mathbb{R}^{N\times N}$ is utilized where $\mathcal{G}_{ij} = 1 \Leftrightarrow$ if an edge$(i, j) \in \mathcal{E}_e$ is physically connected to $\mathcal{MG}_j$, which indicates an edge $(i, j) \in \mathcal{E}_e$ and 0 otherwise. Furthermore, the Laplacian matrix $\mathcal{L} = [l_{ij}] \in \mathbb{R}^{N\times N}$ defined, where $l_{ij} = -g_{ij}$ for $i \neq j$ and the diagonal elements l_{ii} are the sum of all connections for node i, which can represented mathematically as $l_{ii} = \sum_{j=1,j\neq i}^{N} \mathcal{G}_{ij}$. The degree matrix D is also defined as $D = diag\{\mathcal{G}_{11}, \mathcal{G}_{22}, \dots, \mathcal{G}_{NN}\}$.

2.2. Cyber layer

Graph theory provides a practical framework for representing the communication network among MGs in the cluster [10]. The cyber network topology is modeled as an undirected graph, $\mathcal{G}_c(\mathcal{V}, \mathcal{E})$, where each MG in the cluster is represented as a node, and the communication links between MGs are represented as edges. In this network, a cluster of N interacting MGs is defined by the set $\mathcal{V} = \{1, 2, \dots, N\}$ representing each MG, and the edge set $\mathcal{E} \in \mathcal{V} \times \mathcal{V}$, which denotes the communication links between MGs. An edge $(i, j) \in \mathcal{E}$ signifies that $\mathcal{MG}_i$ can receive data from $\mathcal{MG}_j$, emphasizing the direct communication link between them. The network's connectivity can be represented using the adjacent matrix $\mathcal{A} = [\mathcal{G}_{ij}] \in \mathbb{R}^{N\times N}$, where $a_{ij} = 1$ if there is a communication link between $\mathcal{MG}_i$ and $\mathcal{MG}_j$ to exchange data between them, which is mathematically represented by $edge(i, j) \in \mathcal{E}$ and $a_{ij} = 0$ otherwise [17,50]. Additionally, The Laplacian matrix $\mathcal{L}_c = [l_{ij}] \in \mathbb{R}^{N\times N}$ is defined, where $l_{ij} = -a_{ij}$, $i \neq j$, and the diagonal elements l_{ii} are the sum of all connections for node i, which can represented mathematically as $l_{ii} = \sum_{j=1,j\neq i}^{N} a_{ij}$. The degree matrix D is also defined as $diag\{a_{11}, a_{22}, \dots, a_{NN}\}$ [51].

3. Proposal control

The control structure of the MG cluster MGs cluster control involves two levels: the MG control layer, which manages generation within individual DGs as explained in [2] and the cluster control layer, which coordinates generation between MGs are explained in the following subsections:

3.1. The main control objectives

Inspired by [33], the control objectives of the proposed control scheme focus on ensuring proportionate current sharing and average voltage regulation across MGs in the cluster, as expressed in Eqs. (1) and (2). The main objective of current sharing, shown in (1), is to guarantee the ratio of current I_i to its maximum loading capacity I_{ci} for $\mathcal{MG}_i$ converges with that of $\mathcal{MG}_i$:

$$\lim_{t \to T_{Max}} \left(\frac{I_i}{I_{ci}} - \frac{I_j}{I_{cj}} \right) = 0 \qquad \text{for all} \quad i, j \in \mathcal{V}_e \tag{1}$$

where, I_{Ci} and I_{Cj} indicate the maximum loading capacities of $\mathcal{MG}_i$ and $\mathcal{MG}_j$ in the cluster, both of which must be higher than zero. Furthermore, T_{max} represents the maximum convergence time of the cluster currents.

The second control objective, expressed in Eq. (2) is to preserve steady average voltage of each $\mathcal{MG}(\bar{V}dc_i)$ in the cluster, which should be aligned with the reference voltage Vdc_{ref} in steady-state conditions ($\bar{V}dc - Vdc_{ref} = 0$).

$$\bar{V}dc = \frac{1}{n} \sum_{i=1}^{n} Vdc_i = Vdc_{ref} \tag{2}$$

These control objectives are imperative to ensure balanced current allocation and stable voltage regulation in the MGs cluster under varying load conditions and fault scenarios.

3.2. Adaptive distributed fixed-time event-triggered consensus algorithm

An adaptive fixed-time consensus algorithm based on saturation function (sat) has been proposed in this study for the secondary control level as stated in Eq. (3). This is to accomplish a fast speed of DC currents convergence along with less voltage recovery time compared to the fixed time consensus algorithm proposed in [39]. The voltage information can be derived by computing the current error, which subsequently allows for the determination of the reference voltage (V_{ref}) as expressed in Eq. (4). This approach is applied across multiple MGs with a new proposed threshold value that adapts the cluster's conditions, ensuring stable voltage regulation while achieving the desired speed of the DC convergence.

$$\hat{u}_i = ka_1 \; sat(\hat{\varphi}_{Li})^m + ka_2 \; sat(\hat{\varphi}_{Li})^n \tag{3}$$

$$V_{ref} = \Delta V_V + \Delta V_i \tag{4}$$

To ensure precise fixed time stability in the proposed control scheme, the control coefficients m, n are chosen such that m is less than one and n lies between 1 and 2. Additionally, the other control coefficients, ka_1 and ka_2 are set to be adaptive and determined using artificial neural networks (ANN) following the same procedures outlined in section C. The ANN is trained with 35 000 samples of ka_1 and ka_2 and I_{dc} to fine-tune these coefficients, enhancing the performance of the fixed-time consensus algorithm in the secondary control layer to overcome algorithm in [39] . It is important to mention that the maximum convergence time T_{Max} in Eq. (1) can be calculated based on the Eq. (5):

$$T_{max} \leq \frac{1}{ka_1 (1-m)} + \frac{1}{ka_2 (1-n)} \tag{5}$$

According to Eq. (4), the two components of $Vref$ can be calculated based on the available currents at the last triggering instants ($\hat{\varphi}_{Li}$), as expressed in Eq. (6).

$$\hat{\varphi}_{Li} = a_{ij} \sum_{j \in i} \left(\frac{\hat{I}_i(t)}{I_{ci}} - \frac{\hat{I}_j(t)}{I_{cj}} \right) = 0 \qquad \text{where} \quad t \in (t_k^i, t_{k+1}^i) \tag{6}$$

By substituting Eq. (6) into Eq. (3), the estimated current error ($\hat{u}_i$) can be calculated as shown in Eq. (7).

$$\begin{aligned} \hat{u}_i = k_1 \; sat \left(a_{ij} \sum_{j \in i} \left(\frac{\hat{I}_i(t)}{I_{ci}} - \frac{\hat{I}_j(t)}{I_{cj}} \right) \right)^m \\ + k_2 \; sat \left(a_{ij} \sum_{j \in i} \left(\frac{\hat{I}_i(t)}{I_{ci}} - \frac{\hat{I}_j(t)}{I_{cj}} \right) \right)^n \end{aligned} \tag{7}$$

where, $\hat{I}_i$ and $\hat{I}_j$ denote the values of MG currents at the most recent triggering instants. By integrating the Eq. (7) with the gain control (K_i), the current correction factor (ΔV_i) can be determined as demonstrated in Eq. (8).

$$\Delta V_i = K_i \int_0^t \hat{u}_i dt \tag{8}$$

Another component of the voltage reference, which is known as the voltage correction factor (ΔVv) can be obtained by determining the voltage regulation error ($\hat{u}_v$). In this context, the local average voltage ($\hat{\bar{V}}dc_i$) is calculated by combining the local voltage of MG_i with the estimated local voltage error ($\hat{\varphi}v_i$), which is derived by multiplying the gain control (K_t) with the integrated estimated current error($\hat{u}_i$), as shown in Eq. (10). it is noticed that $\hat{\bar{V}}dc_i$ primarily depends on the integrated estimated current error ($\hat{u}_i$) to generate $\hat{\varphi}v_i$. Subsequently, any issue in one of the interconnected MGs in a cluster causes $\hat{u}_i$ to either decrease or increase, which in turn impacts $\hat{\varphi}v_i$, due to the correlation between them, as shown in Eq. (10). this impact on $\hat{\varphi}v_i$, consequently influences $\hat{\bar{V}}dc_i$, as illustrated in Eq. (9), indicating that $\hat{u}_i$ plays a significant role in managing $\hat{\bar{V}}dc_i$.

$$\hat{\bar{V}}dc_i = Vdc_i + \hat{\varphi}_{Vi} \tag{9}$$

$$\hat{\varphi}Vi = K_t \int_0^t \hat{u}_i dt \tag{10}$$

$$\hat{u}_V = \hat{\bar{V}}dc_i + Vdc_{ref} \tag{11}$$

$$\hat{u}_V = (Vdc_i + K_t \int_0^t \hat{u}_i) - Vdc_{ref} \tag{12}$$

$$\Delta V_V = K_V . \hat{u}_V = K_V . \left(Vdc_i + K_t \int_0^t \hat{u}_i \right) - Vdc_{ref} \tag{13}$$

Therefore, both Eqs. (8) and (13) are substituted into Eq. (4) to produce the reference voltage that is sent to the primary control layer of each MG in the cluster, as expressed in Eq. (14).

$$V_{ref} = \left((Vdc_i + K_t \int_0^t \hat{u}_i dt) - Vdc_{ref} \right) K_V + K_i \int_0^t \hat{u}_i dt \tag{14}$$

$$\dot{V}_{ref} = -K_V . \dot{u}_V - K_i . \hat{u}_i \tag{15}$$

3.3. Lyapunov stability

Based on Eq. (15) and using the principle of Lyapunov equation, Eq. (16) can be obtained.

$$\begin{aligned} W = \frac{1}{2} V_{ref}^T L_e V_{ref} \rightarrow \dot{W} = V_{erf}^T L_e \dot{V}_r ef \\ = -I(K_V . \hat{u}_V + K_i . \hat{u}_i) = -(I K_V \hat{u}_V + I K_i \hat{u}_i) \end{aligned} \tag{16}$$

In order to obtain the output current of MG, the error of the current in Eq. (6) can be rearranged to obtain the current as in Eq. (17).

$$I = \frac{\varphi L_i}{L_c I_c^{-1}} \tag{17}$$

The relationship between real-time current sharing error and the event-triggered current sharing error should be derived, as illustrated in

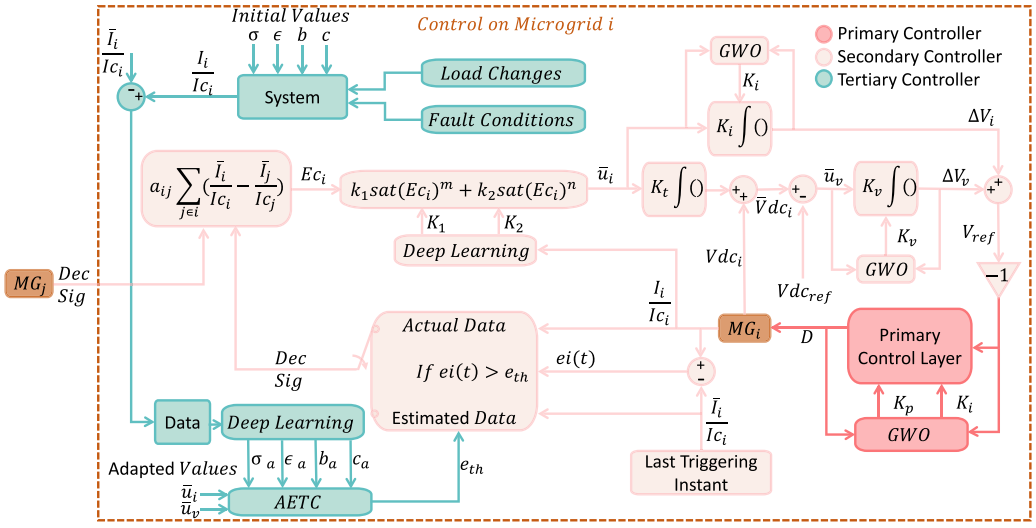

Fig. 2. Proposed control scheme.

Eq. (18).

$$\begin{cases} ei(t) = \frac{I_i(t_{k+1})}{I_{ci}} + \frac{\hat{I}_i(t_k)}{I_{ci}} \rightarrow \frac{\hat{I}_i(t_k)}{I_{ci}} = \frac{I_i(t_{k+1})}{I_{ci}} - ei(t) \\ ej(t) = \frac{I_j(t_{k+1})}{I_{cj}} + \frac{\hat{I}_j(t_k)}{I_{cj}} \rightarrow \frac{\hat{I}_j(t_k)}{I_{cj}} = \frac{I_j(t_{k+1})}{I_{cj}} - ej(t) \end{cases} \tag{18}$$

Then, Substituting Eq. (18) into Eq. (6) produces Eq. (19).

$$\hat{\varphi}_{Li} = a_{ij} \sum_{j \in i} \left(\frac{I_i(t)}{I_{ci}} - ei(t) - \frac{I_j(t)}{I_{cj}} + ej(t) \right) \tag{19}$$

Eq. (19) is further organized and rearranged to make it in terms of the Laplacian matrix so that Eq. (20) can be obtained.

$$\hat{\varphi}_{Li} = \varphi Li - L_c e(t) \rightarrow \hat{\varphi}_{Li} = \varphi Li + L_c e(t) \tag{20}$$

Eq. (20) is substituted into Eq. (17) to obtain Eq. (21), which is then substituted into Eq. (16) to yield Eq. (22).

$$I = \frac{\hat{\varphi}_{Li}}{L_c I_c^{-1}} + \frac{L_c e(t)}{L_c I_c^{-1}} = \frac{\hat{\varphi}_{Li}}{L_c I_c^{-1}} + \frac{e(t)}{I_c^{-1}} \tag{21}$$

$$\begin{aligned} \dot{W} &= -\left(\frac{\hat{\varphi}_{Li}}{L_c I_c^{-1}} + \frac{e(t)}{I_c^{-1}} \right) (K_V \hat{u}_V + K_i \hat{u}_i) \\ &= -K_V \hat{u}_V \frac{\hat{\varphi}_{Li}}{L_c I_c^{-1}} - K_V \hat{u}_V \frac{e(t)}{I_c^{-1}} - K_i \hat{u}_i \frac{\hat{\varphi}_{Li}}{L_c I_c^{-1}} - K_i \hat{u}_i \frac{e(t)}{I_c^{-1}} \end{aligned} \tag{22}$$

Depending on the derived Lyapunov function shown later in the section and a comparison with the root of inequality $\pm xy \leq (\frac{b}{2})x^2 + \frac{1}{2b}y^2$, Eqs. (23) and (24) are obtained:

$$-K_V \hat{u}_V \frac{\hat{\varphi}_{Li}}{L_c I_c^{-1}} \leq \frac{K_V b}{2 L_c I_c^{-1}} \hat{u}_V^2 + \frac{K_V}{2bL_c I_c^{-1}} \hat{u}_i^2 \tag{23}$$

$$-K_i \hat{u}_i \frac{\hat{\varphi}_{Li}}{L_c I_c^{-1}} \leq \frac{K_i}{2 L_c I_c^{-1}} \hat{u}_i^2 \tag{24}$$

For a seek of simplicity, $\hat{\varphi}_{Li}$ is assumed to be $\hat{u}_i$

$$-K_V \hat{u}_V \frac{e(t)}{I_c^{-1}} \leq \frac{K_V b}{2 I_c^{-1}} \hat{u}_V^2 + \frac{K_V}{2bI_c^{-1}} e(t)^2 \tag{25}$$

$$\frac{e(t)}{I_c^{-1}} K_i \hat{u}_i \leq \frac{K_i b}{2 I_c^{-1}} \hat{u}_i^2 + \frac{K_i}{2bI_c^{-1}} e(t)^2 \tag{26}$$

Eqs. (23)–(26) are then substituted into Eq. (22) to obtain Eq. (27).

$$\begin{aligned} \dot{W} \leq{}& \frac{K_V b}{2 L_c I_c^{-1}} \hat{u}_V^2 + \frac{K_V b}{2bL_c I_c^{-1}} \hat{u}_i^2 + \frac{K_V b}{2 I_c^{-1}} \hat{u}_V^2 \\ &+ \frac{K_V}{2bI_c^{-1}} e(t)^2 + \frac{K_i b}{2 I_c^{-1}} \hat{u}_i^2 + \frac{K_i}{2bI_c^{-1}} e(t)^2 + \frac{K_i}{2 L_c I_c^{-1}} \hat{u}_i^2 \end{aligned} \tag{27}$$

By rearranging Eq. (27), the Lyapunov function can be obtained as follows (see Eq. (28)):

$$\begin{aligned} \dot{W} \leq{}& \left(\frac{K_V b}{2 L_c I_c^{-1}} + \frac{K_V b}{2 I_c^{-1}} \right) \hat{u}_V^2 + \left(\frac{K_V b}{2bL_c I_c^{-1}} + \frac{K_i b}{2 I_c^{-1}} + \frac{K_i}{2 L_c I_c^{-1}} \right) \hat{u}_i^2 \\ &+ \left(\frac{K_V}{2bI_c^{-1}} + \frac{K_i}{2bI_c^{-1}} \right) e(t)^2 \end{aligned} \tag{28}$$

From Eq. (28), the new threshold value of the error can be assumed to be as follows (see Eq. (29)):

$$e(t)^2 \geq \frac{\left(\frac{K_V b}{L_c} + \frac{K_V b}{1} \right) \hat{u}_V^2 + \left(\frac{K_V}{bL_c} + \frac{K_i b}{1} + 2\frac{K_i}{L_c} \right) \hat{u}_i^2}{\left(\frac{K_V + K_i}{b} \right)} \tag{29}$$

Eq. (29) can be further organized to obtain Eq. (30).

$$e(t)^2 \geq \sigma_a \left(\frac{K_V b_a + L_c K_V b_a}{\frac{K_V + K_i}{b} L_c} \right) \hat{u}_V^2 + \sigma_a \left(\frac{K_V + L_c K_i b_a^2 + 2K_i b_a}{(K_V + K_i) L_c} \right) \hat{u}_i^2 \tag{30}$$

In Eq. (30), a state-dependent function (SDF) is derived. By combining the best features of SDF and the time-dependent triggered function (TDF), a mixed-dependent function (MSTDF) is achieved. The MSTDF protocol efficiently prevents excessive triggering by enforcing a minimum interevent time, thereby eliminating Zeno behavior, which occurs when the time between events reaches zero and causes event-triggered methodologies to fail. Compared to other triggering methods, MSTDF has been shown to provide a superior performance with the fewest total events [52]. To leverage the benefits of this protocol, a time-dependent term is

$$\begin{aligned} e(t)^2 \geq{}& \sigma_a \left(\frac{K_V b_a + L_c K_V b_a}{\frac{K_V + K_i}{b} L_c} \right) \hat{u}_V^2 \\ &+ \sigma_a \left(\frac{K_V + L_c K_i b_a^2 + 2K_i b_a}{(K_V + K_i) L_c} \right) \hat{u}_i^2 + c e^{-\rho t} \end{aligned} \tag{31}$$

The value of σ_a, b_a, ρ_a and c_a are selected based on the cluster conditions in Fig. 2 using artificial neural networks (ANN). In the previous studies, these coefficients were fixed, increasing the probability of Zeno behavior. However, in this study, all coefficients are chosen to be positive and span a wide range of values, as explained in Section 3. This contributes to reducing the frequency of events, thereby eliminating Zeno behavior.

3.4. ANN implementation

This section investigates the influence of σ_a, b_a, c_a, and ρ_a in Eq. (31) on communication across MGs in a cluster with and without ANN to determine the viability of using ANN to predict these coefficients under various operating situations. For the instance where ANN was not used, various scenarios with random control coefficient values were tested. It was discovered that reducing the values of these parameters increases the MAECT's sensitivity to minor errors in the cluster, indicating more needless interactions occur. As the values of these coefficients increase, the cluster becomes less susceptible to errors, which may reduce the dependability of communication if necessary. In real-life circumstances, faults and loading conditions are unpredictable; hence, adopting fixed values for these parameters might result in the cluster being unable to tackle these conditions. In this study, 1,046,000 simulated samples of σ_a, b_a, c_a, and ρ_a with the error that results from differences between actual and estimated values of the currents in the DC MGs cluster, which have been collected from the simulated cluster under different load and faults conditions, have been used to train ANN. The nature of these variables is essential to our research since they directly impact the ANN's ability to simulate the link between the error and the necessary control coefficient adjustments required for the secure and effective operation of the interaction among MGs in the cluster. The Levenberg–Marquardt algorithm has been used to train the ANN, allocating 70% of the data to learning, 15% to testing, and 15% to validation. A feed-forward neural network was constructed in MATLAB with a single hidden layer of 10 neurons to model this relationship. It has been trained with 1,046,000 datasets, adjusting the weights and biases to reduce errors over 1000 epochs. After training, the accuracy of the network is evaluated by calculating the mean square error between the predicted outputs and the actual targets.

This figure shows the structure of physical and cyber layers. The physical layer includes MGs in a cluster and the tie-lines linking them as illustrated in Fig. 1. Each MG has two distributed generation units (DGs) as shown in Fig. 3. The cyber control layer comprises three main parts, primary, secondary and tertiary control layers of the hierarchical control scheme. The primary control layer, which is further illustrated in Fig. 2, includes dual control loops to regulate the voltage and current of each MG in a cluster. Also, the secondary control layer which applies an adaptive fixed time consensus algorithm with GWO, as explained in Fig. 2 to minimize the voltage deviation and enhance currents convergence in a cluster. The third is the tertiary control layer, which use an adaptive event-triggered consensus algorithm based on Artificial neural networks to effectively manage interactions among the MGs in a cluster, as illustrated in Fig. 3.

3.5. GWO implementation

In this paper, Gray Wolf Optimizer (GWO), discussed in [53], and noted for its fast convergence, simplicity, and easy implementation [44] is used to optimize the parameters of PI controllers in the secondary control layer, as shown in Fig. 2. This optimization approach improves current sharing and global voltage regulation within the DC MGs cluster (DCMGC). The fitness function used is defined in Eq. (32) as follows:

$$ITAE = \int_0^{\infty} t|\hat{u}(t)|dt \tag{32}$$

$$\hat{u}_V = \hat{\bar{V}}dc_i - Vdc_{ref} \tag{33}$$

$$\hat{u}_i = ka_1\ sat(\hat{\varphi}_{Li})^m + ka_2\ sat(\hat{\varphi}_{Li})^n \tag{34}$$

ITAE minimization is commonly used as a criterion for tuning the parameters of PI controllers, as discussed in [54]. The methodology behind the proposed control strategy is explained in algorithm 1.

Algorithm 1 Gray Wolf Optimizer for Tuning PID Coefficients

begin
  Initialize the population of grey wolves X_i $(i = 1, 2, \ldots, n)$
  Set the parameters a, A, and C
  Calculate the fitness of each search agent
  Assign X_α = as the best search agent
  Assign X_β = as the second best search agent
  Assign X_δ = as the third best search agent
  while stopping criterion not met **do**
    for each search agent **do**
      for each dimension **do**
        Update the position of the current search agent using:

$$D_\alpha = |C_1 \cdot X_\alpha - X| \quad D_\beta = |C_2 \cdot X_\beta - X| \quad D_\delta = |C_3 \cdot X_\delta - X|$$

$$X_1 = X_\alpha - A_1 \cdot D_\alpha \quad X_2 = X_\beta - A_2 \cdot D_\beta \quad X_3 = X_\delta - A_3 \cdot D_\delta$$

$$X = \frac{X_1 + X_2 + X_3}{3}$$

      end for
    end for
    Update a, A, and C
    Evaluate the fitness of each search agent
    Update X_α, X_β, and X_δ
  end while
end

4. Results and discussion

In this study, a four DC-MG cluster, shown in Fig. 1, is adopted and simulated in MATLAB to evaluate the effectiveness of the proposed control scheme compared to existing control schemes. In this study, the MGs are connected by tie lines with 1 Ω resistances. It is worth mentioning that each MG has two distributed generation units (DGs) placed in tandem. Additionally, DC-DC buck converters are employed to achieve an output voltage of 48 V for the MG loads. Fig. 3 illustrates the main components of each MG in the cluster, while specifications of DC MG are provided in Table 1. Communicatively, it is noticed that each MG's controller exchanges local information with neighboring MGs, as shown in Fig. 1. This interaction allows the deriving the Laplacian matrix as follows:

$$\mathcal{L}_e = \begin{bmatrix} G11 & G12 & G13 & G14 \\ G21 & G22 & G23 & G24 \\ G31 & G32 & G33 & G34 \\ G41 & G42 & G43 & G44 \end{bmatrix} = \begin{bmatrix} 2 & -1 & -1 & 0 \\ -1 & 2 & 0 & -1 \\ -1 & 0 & 2 & -1 \\ 0 & -1 & -1 & 2 \end{bmatrix} \tag{35}$$

The control layer of each MG consists of the primary control layer, as depicted in Fig. 3. It is noticed that the reference voltage (V_{ref}) from the secondary efficiently adjusts the DC bus voltage and current levels of each MG in the cluster. In this respect, the voltage loop regulates the output voltage based on measured (V_{dc}) voltage and reference voltage, while the current loop adjusts the output current using measured current (I_{dc}) and reference current (I_{ref}). These control loops assist the primary control layer to achieve the MG's primary control objectives: maintaining stable output voltage and synchronizing the MG's output power with the load demands. This control scheme ensures the overall stability and reliability of the MGs, guaranteeing efficient fulfillment of the load's power requirements.

4.1. Simulation results

In this section Disturbances and faults have been applied in both physical and cyber layers.

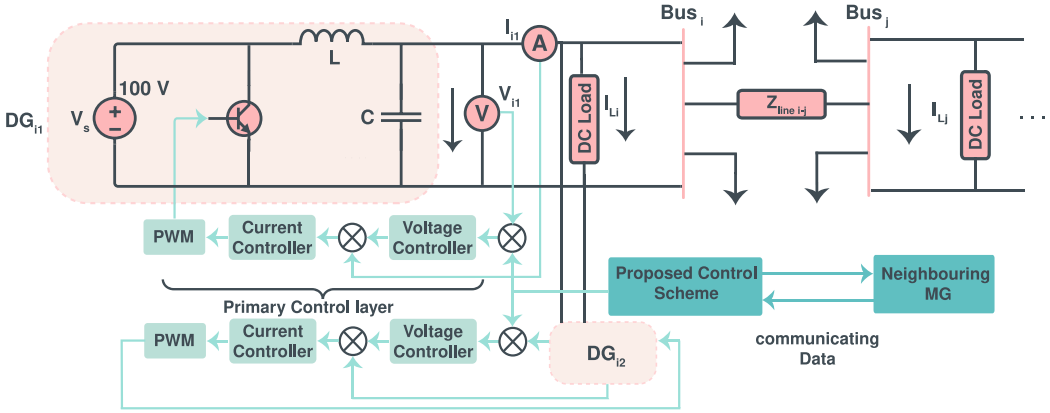

Fig. 3. The structure of each MG inside MGC.

Table 1
MGs Parameters.

Symbol	Value	unit
Nominal Voltage	48	V
Converter Resistance	0.52	Ω
Converter Inductor	0.002	H
Converter Capacitor	0.005	F
Switching Frequency	20,000	Hz
K_i and K_V	Optimized	——
Conductance	1.25	S

4.1.1. Physical layer disturbances

In this research, the load resistances of the MGs in Fig. 1 are set to 24 Ω, 12 Ω, 16 Ω, and 9.6 Ω, each operating at a nominal voltage of 48 Ω. These specific load values have been selected to ensure a fair and consistent comparison with the study presented in Ref. [34]. By adopting identical load conditions, the robustness and performance of the proposed control method can be effectively demonstrated under comparable scenarios. The adjacent MGs, with rated currents of 8 A and 10 A, quickly converge to the equilibrium point within 0.02 s – enormously faster than previous studies, such as those reported in [34], as exhibited in Fig. 4(a). Obviously, the load currents stabilize at values of 3.1 A, 3.1 A, 3.9 A, and 3.9 A, emphasizing the effectiveness of the control strategy in guaranteeing accurate proportional current sharing among the MGs in the cluster based on their maximum capacity ratings. Regardless of these different load conditions, the DC bus voltages are kept within an acceptable range of 48.45 V to 47.54 V, as illustrated in Fig. 5(a).

To further evaluate this control scheme, the MGs' DC loads are changed at 1.5 s and 2.5 s, increasing the overall DC load current from 13.9 A to 22.4 A and 28.4 A, respectively. In order to assess the robustness of this control scheme under simultaneous load changes and fault conditions, this control scheme also has been tested by applying a short-circuit fault with a rating of 3.5 Ω to MG2 at 1 s and to MG3 at 2 s. It is noticed that the cluster responds promptly to these simultaneous conditions, as exhibited in Fig. 8. It is also noticed that the DC bus voltages remain well-regulated at 48.38 V, 48.36 V, 47.7 V, and 47.62 V between 1 s and 2.5 s. Furthermore, the load currents achieve steady values at 1.5015 s and 1.502 s for the 1.5 s–2.5 s period, respectively, as illustrated in Fig. 4.

Likewise, during steady-state operations, the average DC bus voltage in the MG is constantly regulated within an acceptable range (47.95 V to 48.018 V), promptly returning to normal levels after disturbances at 1 s, 1.5 s, 2 s, and 2.5 s, as shown in Fig. 5(b). Also, the voltage tracking errors (VTE), indicating deviations of the DC bus voltages from the reference voltages, remain within the lowest range (0.98 V to −0.71 V) during these disturbances, as demonstrated in Fig. 5(c). Therefore, as defined in Eqs. (1) and (2), the main control objectives are accurately realized as explained in Figs. 5(c), 5(d), and 5(b). The number of triggering events is significantly decreased compared to previous studies, as illustrated in Fig. 6(a). This reduction is attributed to the insignificant cluster errors, which infrequently exceed the threshold value in Eq. (31) during load changes and faults conditions due to the adaptive determination of the control coefficients in Eq. (31) based on ANN. This validates the resilience of the proposed control scheme in Fig. 2 against insignificant errors that do not have considerable influences on the communication among MGs, as observed in Fig. 6(b). Fig. 6(a) illustrates that the frequency of data sampling and transmission is substantially reduced to only 20 instances at millisecond intervals.

To conclude, Figs. 4–5 illustrate the feasibility of the proposed control strategy in preserving voltage regulation within a range of 1.04 to 1.3% across MGs, guaranteeing accurate current sharing and excluding the unnecessary interactions amongst MGs in the cluster. This influences considerably lowering the probability of data congestion, as the control scheme facilitates DC MGs within the cluster to operate efficiently with minimal need for continuous and large-scale data exchange, as shown in Fig. 6(a). These results shows the effectiveness of the proposed control strategy in achieving accurate coordination among MGs in the cluster. As illustrated in Fig. 6(a), AMDETC decreases the communication updates among MGs in the cluster by establishing a minimum time threshold between events.

4.1.2. Cyber layer disturbances

In this section different scenarios have been simulated to assess the robustness control scheme under critical disturbances occurring in the cyber layer, including communication delay, communication fault, network disturbance, and data transmission issues.

First Scenario:

In the first scenario, communication delay conditions, are applied to the cluster in Fig. 1 to evaluate its performance under such critical conditions. The same load changes in the first subsection are reapplied with simulated communication delay of 35 ms introduced in MG1. The simulation results demonstrate that, although the 35 ms communication delay, the proposed controller accomplishes proportional load current sharing as, illustrated in Figs. 7(a) & 7(b). It also effectively retains both local voltages and the average voltages of the MGs in the cluster at the standard value, as shown in Figs. 7(c) & 7(d) . However, when the delay increases to more than 40 ms, voltage and current oscillations begin to occur, indicating that further delay may lead to may cause the system instability.

Second Scenario:

In the second scenario, the proposed control scheme has been tested under simultaneous cyber layer issues such as a network disturbance in MG1 at 0.5 s, a communication fault in MG3 at 1.7 s, and data transmission issues in MG4 at 3.1 s, in addition to previously tested

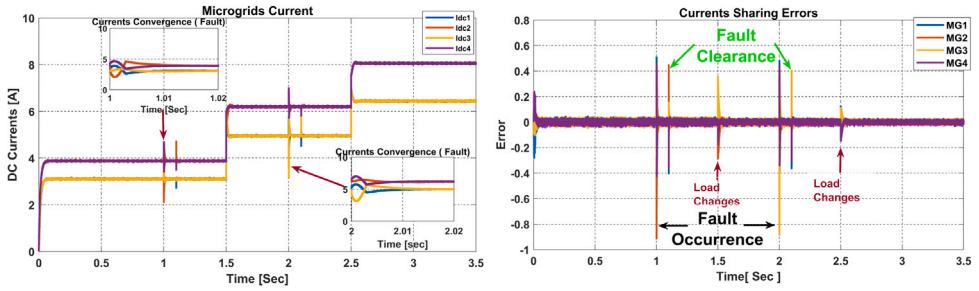

(a) DC Current (b) Current Sharing errors

Fig. 4. Physical layer, Scenario I&II in Eq. (1).

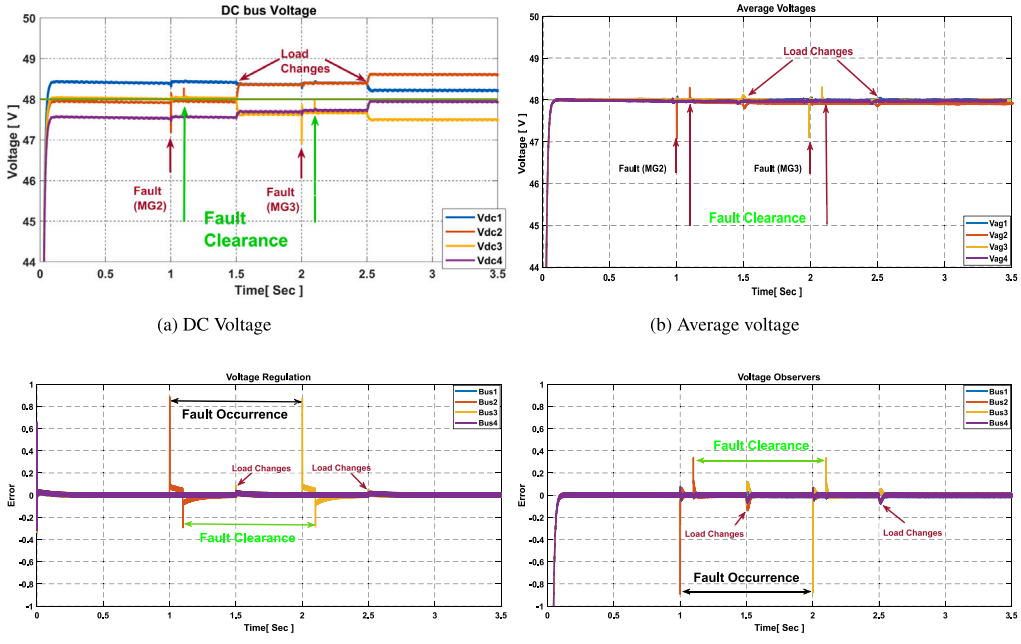

(a) DC Voltage (b) Average voltage

(c) Voltage regulation errors (d) Voltage observers

Fig. 5. Physical layer, Scenario I&II in Eq. (2).

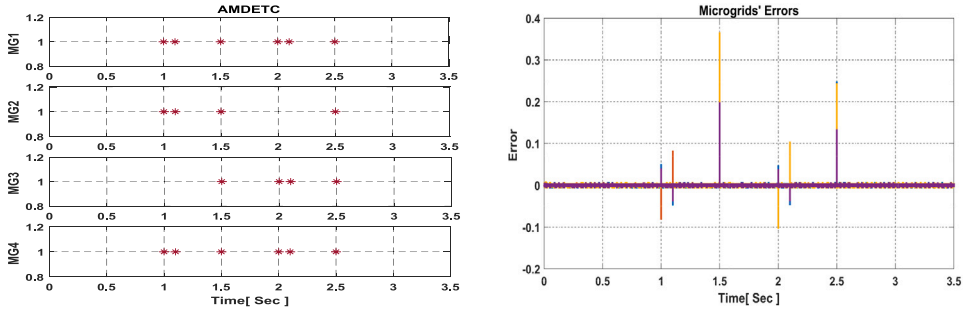

(a) Triggering instants for each MG in the cluster. (b) MG's currents errors

Fig. 6. The proposed control performance.

physical layer disturbances. It is noticed that the cluster responds promptly to these combined conditions and return to normal operation after the disturbances are cleared from the cluster. it is found that the proposed control scheme achieves the control objectives in Eq. (1), by ensuring accurate proportional current sharing among the MGs in the cluster, as illustrated in Fig. 8. Additionally control objective in Eq. (2) is fulfilled by promptly restoring the local voltages and average voltages to normal levels after disturbances, as shown in Fig. 9. This verifies the robustness of the proposed control scheme and its sustainability for real-life applications.

4.2. OPAL-RT validation

In order to validate the suitability of the proposed control scheme in real-life scenarios, real-time simulations, which play a vital role in evaluating the effectiveness of the proposed controllers, can be adopted. This is because the models employed in real-time simulations can be operated effectively at the same frequency as the physical system [55]. To accomplish this, the OPAL-RT simulator cooperates with Matlab/Simulink via RT-LAB software installed on a host com-

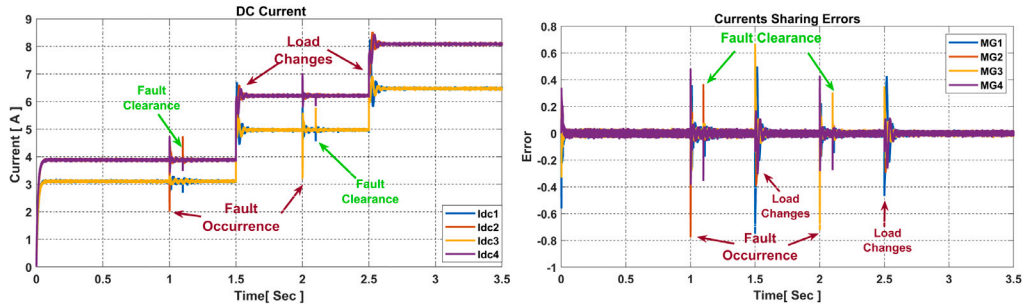

(a) DC Current (b) Currents Sharing Errors

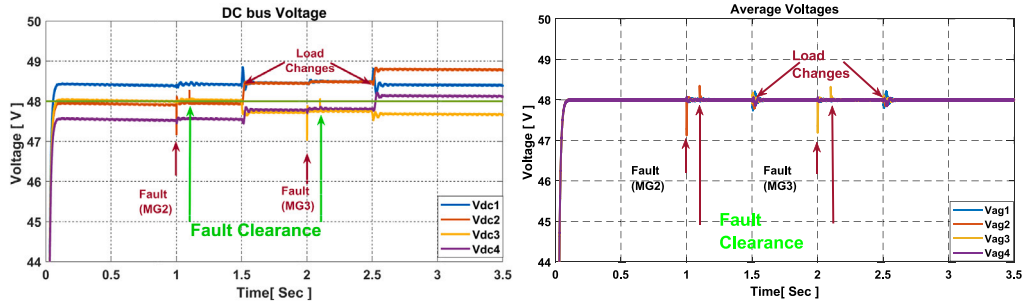

(c) DC Voltage (d) Average voltage

Fig. 7. Cyber Physical layer, Scenario I.

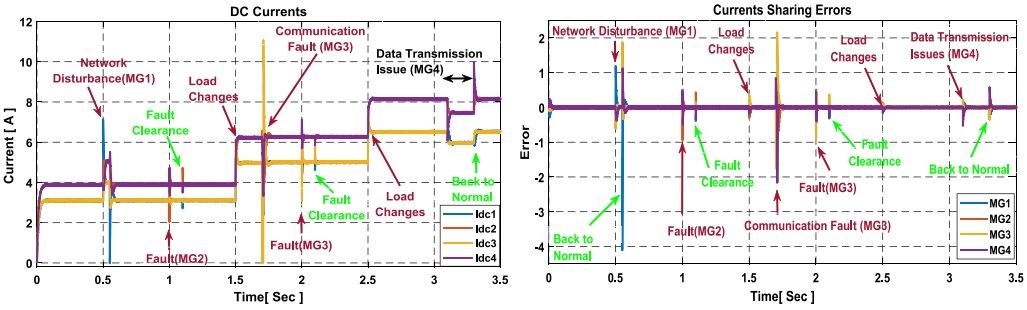

(a) DC Current (b) Currents Sharing Errors

Fig. 8. Cyber Physical results, Scenario II: (a) DC current and (b) Current sharing errors.

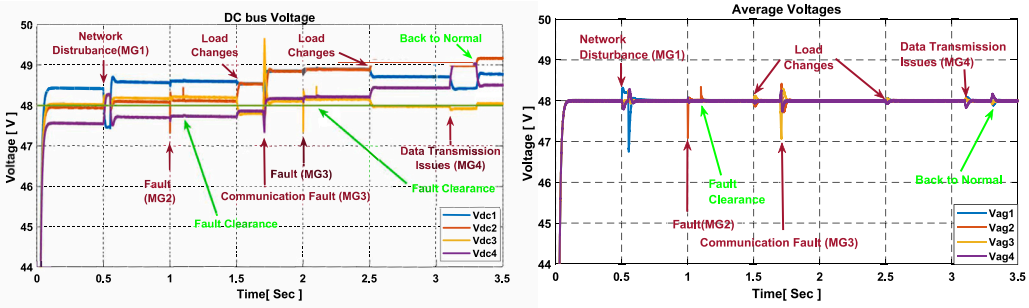

(a) DC Voltage (b) Average voltage

Fig. 9. Cyber Physical results, Scenario II: (a) DC voltage and (b) Average voltage.

puter. In this paper, the performance of the proposed control strategy is evaluated through real-time simulation, focusing on current convergence, DC bus voltage regulation, and data exchange among MGs during unexpected disturbances within the cluster. Fig. 10 exhibits the complete laboratory setup, which includes an OP5700 simulator, a host computer, and a Micsig digital storage oscilloscope. The proposed control approach is tested under specific scenarios, such as load variations across all cluster MGs and simultaneous faults in MG2 and MG3. It is found that the control strategy achieves fewer interactions between MGs in the cluster, maintains a constant DC bus voltage, and ensures efficient sharing of current across the MGs under different operating conditions in real time, which confirms that real-time simulations validate the proposed control approach, demonstrating synchronization with real-time operations as shown in Fig. 12.

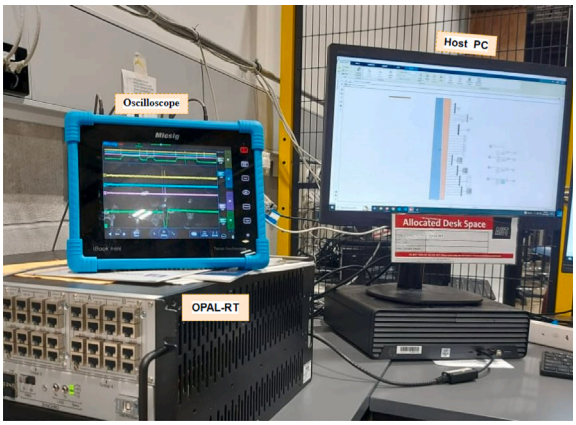

Fig. 10. Experiment set-up in OPAL-RT.

To conclude, it is obvious that the results of the Opal-RT simulations validate the MATLAB simulation results in Section 4. It is visible that DC voltages are quickly recovered after simultaneous load changes and faults at MG2 and MG3, as shown in Fig. 12, and DC currents are quickly converged to their equilibrium points, as revealed in Figs. 11(a) and 11(b). In addition, the accuracy of the triggered instants is 100%, as obtained in the MATLAB simulations, which indicates that unnecessary communication among the MGs in the cluster has been eliminated, as demonstrated in Fig. 12(d). Based on the MATLAB simulation and OPAL-RT results, it is obvious that the proposed control scheme is highly suitable for real-life scenarios.

5. Comparison with the existing control techniques

In order to evaluate this approach as compared with existing control schemes in the literature, DC voltages regulation, the speed of DC currents convergence, and the need of communication among MGs under steady and emergency states are taken in consideration. In this study, the proposed control strategy is compared to the Distributed Event-Triggering Consensus Algorithm (DETC) mentioned in [34] and the Mixed Time-State Dependent Distributed Event-Triggering Consensus Protocol (MDETC).

The integration of Grey Wolf Optimizer (GWO) in the secondary control layers of the proposed control scheme ensures voltage regulation within the range of 47.62 V to 48.38 V from 1.5 s to 2.5 s. In contrast, the DC bus voltage range in [34] was recorded as 47.1 V to 49.5 V at 1.5 s and 42.8 V to 51.76 V at 2.5 s. Furthermore, DC current convergence occurred at 0.01 s after faults at MG2 and MG3, which is quicker than the control approach in [34], as illustrated in Fig. 4 . Also, more accurate current sharing among MGs in the cluster has been attained compared to [34]. Furthermore, the proposed control scheme significantly reduces triggering instances compared to [34] and MDETC. Specifically, it requires 20 instances **(6, 4, 4, and 6)** as shown in Fig. 6(a) versus 201 instances (45,46,59,51) required by DETC in [34] and 88 instances **(22, 19, 24, and 23)** required by MDETC. This reduction, as shown in Fig. 13, exhibits the robustness of the proposed Adaptive event-trigger function in Eq. (31) in minimizing events frequency, which is crucial for preventing Zeno behavior. By maintaining a positive minimum interevent time, the proposed control approach effectively excludes Zeno behavior, enhancing communication efficiency and overall cluster performance more efficiently in transient and steady-state conditions.

The comparison in Fig. 14 shows that the MDETC notably outperforms the distributed event-triggered consensus algorithm in [34] and MDETC in decreasing communication needs among MGs in the cluster, with only 88 instants required compared to 201 and 88, respectively. This affirms the effectiveness of the proposed control technique in improving the whole cluster's effectiveness by reducing data congestion.

This control scheme represents a holistic design by encompassing contributions in the three control layers of the hierarchical control scheme. All PI controllers in the primary layer have been optimized based on GWO to enhance the performance of the individual MGs. The secondary control layer applies hybrid GWO-AFTCA algorithm to ensure the cluster can withstand sudden changes, minimize voltage deviations and realize more accurate currents sharing among MGs. In the third layer, control parameters for the event-triggered condition depicted in Eq. (31) is dynamically adjusted over time based on the cluster conditions, distinguishing this control approach from previous studies in the literature, and this make it more realistic. This strategy manages interactions among MGs in a cluster effectively and remains robust against minor errors, overcoming the limitations of previous studies in the literature. However, this control strategy requires extensive dataset for significant accuracy, which may not always be available. Also, this article focuses the data frequency rather the amount of data, which is an important factor in the large clusters. Therefore, future research should focus on addressing these issues and apply it on a cluster with renewable energy resources. Furthermore, this control scheme needs to be examined under cyber-attacks such as False data injection.

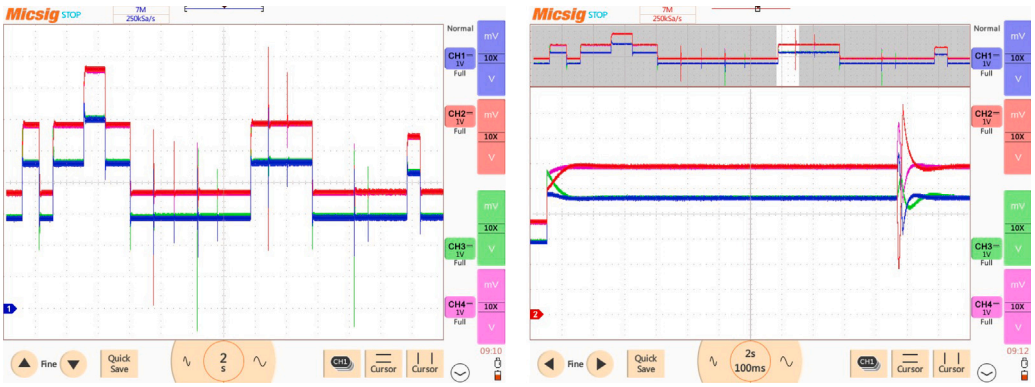

(a) DC Currents under load changes and faults condition.

(b) DC currents convergence after load changes and faults.

Fig. 11. DC current changes of MGs.

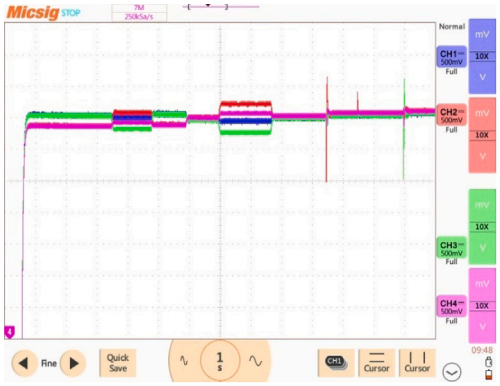

(a) DC voltage under load changes and faults.

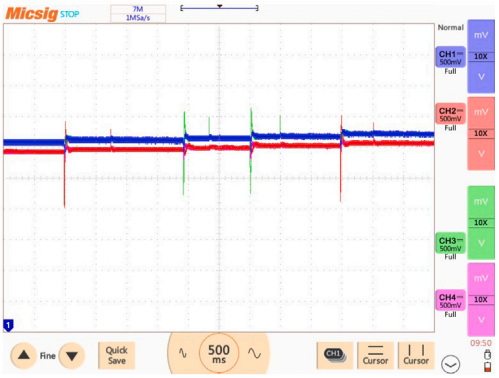

(b) DC voltage under faults at MG2 and MG3.

(c) DC voltages recovery after fault condition.

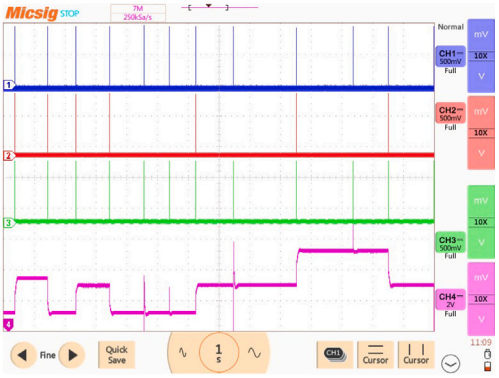

(d) Triggering instances of MG1, MG3, and MG4 with Idc2 after load changes and faults at MG2.

Fig. 12. DC voltages changes and triggers of MGs.

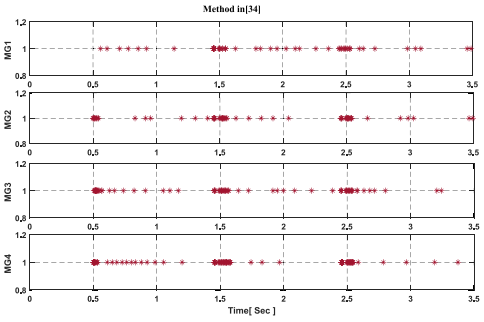

(a) Triggering instants of method in [34]

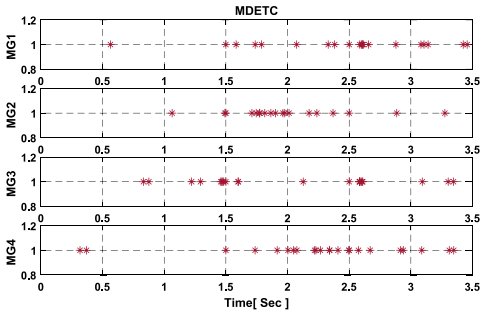

(b) Triggering instants of MDETC.

Fig. 13. Triggering instants of method in [34] and MDETC respectively.

6. Conclusion

This paper presents the Adaptive Mixed Time-State Dependent Distributed Event-Triggered Consensus Protocol (AMDETC) as a novel control approach to enhance the performance of the global control layer in a four-DC MG cluster. The feasibility of the proposed control technique has been successfully validated under disturbances such as simultaneous load changes and fault conditions in the MATLAB environment and OPAL-RT. The simulation results reveal that the adoption of the grey wolf optimizer (GWO) and an adaptive fixed-time consensus algorithm in the secondary control layer of the hierarchical control scheme effectively sustains DC bus voltages within normal boundaries, facilitates speedy recovery from voltage drops, and realizes accurate proportional current sharing based on the maximum loading capacities among the MGs, with swift convergence rates within the cluster. Furthermore, AMDETC imposes strict triggering constraints, reducing the MGs' sensitivity to insignificant errors and minimizing the need for constant interactions among MGs in a cluster, thus reducing the possibility of communication delays. The Simulation and OPAL-RT results confirm the cluster's resilience to disturbances, validating the effectiveness of the proposed control method.

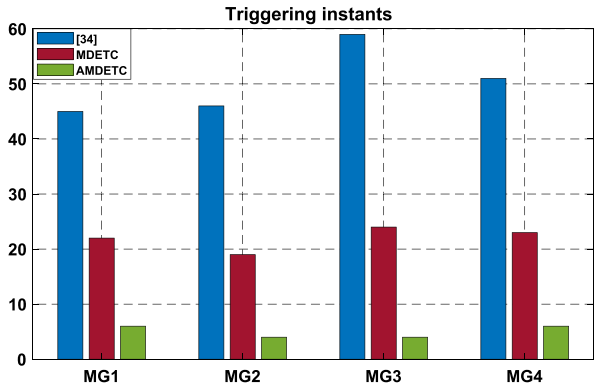

Fig. 14. Comparison between the proposed control method and technique in [34].

CRediT authorship contribution statement

Zaid Hamid Abdulabbas Al-Tameemi: Writing – original draft, Validation, Software, Methodology, Investigation, Conceptualization. **Rasool Peykarporsan:** Writing – review & editing, Visualization, Validation, Investigation, Conceptualization. **Tek Tjing Lie:** Writing – review & editing, Visualization, Supervision, Investigation, Formal analysis, Conceptualization. **Ramon Zamora:** Writing – review & editing, Visualization, Supervision, Investigation, Conceptualization. **Frede Blaabjerg:** Writing – review & editing, Supervision, Investigation, Conceptualization.

Declaration of competing interest

The authors declare the following financial interests/personal relationships which may be considered as potential competing interests: Zaid Al-Tameemi reports financial support was provided by Al-Furat Al-Awsat Technical University. If there are other authors, they declare that they have no known competing financial interests or personal relationships that could have appeared to influence the work reported in this paper.

Acknowledgments

The authors would like to thank Al-Furat Al-Awsat Technical University, Iraq for their financial support in conducting this research. They would also like to note that this study is a part of the MBIE SSIF AETP program entitled Future Architecture of the Network, New Zealand.

Data availability

Data will be made available on request.

References

[1] Q. Xu, Y. Xu, Z. Xu, L. Xie, F. Blaabjerg, A hierarchically coordinated operation and control scheme for DC microgrid clusters under uncertainty, IEEE Trans. Sustain. Energy 12 (1) (2020) 273–283.

[2] Z.H.A. Al-Tameemi, T.T. Lie, G. Foo, F. Blaabjerg, Optimal power sharing in DC microgrid under load and generation uncertainties based on GWO algorithm, in: 2021 IEEE PES Innovative Smart Grid Technologies-Asia (ISGT Asia), IEEE, 2021, pp. 1–5.

[3] O. Rezaei, O. Mirzapour, M. Panahazari, H. Gholami, Hybrid ac/dc provisional microgrid planning model considering converter aging, Electricity 3 (2) (2022) 236–250.

[4] S.K. Sahoo, A.K. Sinha, N. Kishore, Control techniques in AC, DC, and hybrid AC–DC microgrid: A review, IEEE J. Emerg. Sel. Top. Power Electron. 6 (2) (2017) 738–759.

[5] Y. Han, Y. Pu, Q. Li, W. Fu, W. Chen, Z. You, H. Liu, Coordinated power control with virtual inertia for fuel cell-based DC microgrids cluster, Int. J. Hydrog. Energy 44 (46) (2019) 25207–25220.

[6] Z.H.A. Al-Tameemi, T.T. Lie, G. Foo, F. Blaabjerg, Control strategies of DC microgrids cluster: A comprehensive review, Energies 14 (22) (2021) 7569.

[7] K.T. Saraswathi, G.V. Swaminathan, S. Periasamy, Hybrid power management for DC microgrid cluster, Electr. Power Syst. Res. 199 (2021) 107454.

[8] L. Meng, Q. Shafiee, G.F. Trecate, H. Karimi, D. Fulwani, X. Lu, J.M. Guerrero, Review on control of DC microgrids and multiple microgrid clusters, IEEE J. Emerg. Sel. Top. Power Electron. 5 (3) (2017) 928–948.

[9] A. Abhishek, S. Devassy, S. Akbar, B. Singh, Consensus algorithm based two-level control design for a DC microgrid, in: 2020 IEEE International Conference on Power Electronics, Smart Grid and Renewable Energy (PESGRE2020), IEEE, 2020, pp. 1–6.

[10] S. Moayedi, A. Davoudi, Distributed tertiary control of DC microgrid clusters, IEEE Trans. Power Electron. 31 (2) (2015) 1717–1733.

[11] C. Wu, X. Hou, Y. Wang, X. Chen, C. Liao, SOC-featured distributed tertiary control for energy management in DC microgrid clusters, in: 2019 22nd International Conference on Electrical Machines and Systems, ICEMS, IEEE, 2019, pp. 1–4.

[12] Q. Shafiee, T. Dragičević, J.C. Vasquez, J.M. Guerrero, Hierarchical control for multiple DC-microgrids clusters, IEEE Trans. Energy Convers. 29 (4) (2014) 922–933.

[13] R. Babazadeh-Dizaji, M. Hamzeh, Distributed hierarchical control for optimal power dispatch in multiple DC microgrids, IEEE Syst. J. 14 (1) (2019) 1015–1023.

[14] A.A. Mohamed, A.T. Elsayed, T.A. Youssef, O.A. Mohammed, Hierarchical control for DC microgrid clusters with high penetration of distributed energy resources, Electr. Power Syst. Res. 148 (2017) 210–219.

[15] Z. Luo, H. Geng, G. Zhu, Hierarchical cooperative control for islanded DC microgrid cluster, in: 2018 IEEE International Power Electronics and Application Conference and Exposition, PEAC, IEEE, 2018, pp. 1–5.

[16] K. Bharath, M.M. Krishnan, P. Kanakasabapathy, A review on DC microgrid control techniques, applications and trends, Int. J. Renew. Energy Res 9 (3) (2019) 1328–1338.

[17] L. Ding, Q.-L. Han, X. Ge, X.-M. Zhang, An overview of recent advances in event-triggered consensus of multiagent systems, IEEE Trans. Cybern. 48 (4) (2017) 1110–1123.

[18] Z.-G. Wu, Y. Xu, R. Lu, Y. Wu, T. Huang, Event-triggered control for consensus of multiagent systems with fixed/switching topologies, IEEE Trans. Syst. Man, Cybern.: Syst. 48 (10) (2017) 1736–1746.

[19] D. Pullaguram, S. Mishra, N. Senroy, Event-triggered communication based distributed control scheme for DC microgrid, IEEE Trans. Power Syst. 33 (5) (2018) 5583–5593.

[20] Z. Zhang, C. Dou, D. Yue, B. Zhang, S. Xu, T. Hayat, A. Alsaedi, An event-triggered secondary control strategy with network delay in islanded microgrids, IEEE Syst. J. 13 (2) (2018) 1851–1860.

[21] W. Meng, X. Wang, S. Liu, Distributed load sharing of an inverter-based microgrid with reduced communication, IEEE Trans. Smart Grid 9 (2) (2016) 1354–1364.

[22] C. Li, X. Yu, W. Yu, T. Huang, Z.-W. Liu, Distributed event-triggered scheme for economic dispatch in smart grids, IEEE Trans. Ind. Informatics 12 (5) (2015) 1775–1785.

[23] Y. Fan, G. Hu, M. Egerstedt, Distributed reactive power sharing control for microgrids with event-triggered communication, IEEE Trans. Control Syst. Technol. 25 (1) (2016) 118–128.

[24] J. Savaliya, K. Patel, A. Mehta, Distributed event-triggered sliding mode control for voltage synchronization of DC microgrid using leader–follower consensus protocol, in: Advances in Control Systems and Its Infrastructure: Proceedings of ICPCCI 2019, Springer, 2020, pp. 25–35.

[25] S.A. Alavi, K. Mehran, Y. Hao, A. Rahimian, H. Mirsaeedi, V. Vahidinasab, A distributed event-triggered control strategy for DC microgrids based on publish-subscribe model over industrial wireless sensor networks, IEEE Trans. Smart Grid 10 (4) (2018) 4323–4337.

[26] Z. Li, Z. Cheng, J. Si, S. Li, Distributed event-triggered secondary control for average bus voltage regulation and proportional load sharing of DC microgrid, J. Mod. Power Syst. Clean Energy 10 (3) (2021) 678–688.

[27] P. Shafiee, Y. Khayat, Y. Batmani, Q. Shafiee, J.M. Guerrero, On the design of event-triggered consensus-based secondary control of DC microgrids, IEEE Trans. Power Syst. 37 (5) (2022) 3834–3846.

[28] B. Fan, J. Peng, Q. Yang, W. Liu, Distributed periodic event-triggered algorithm for current sharing and voltage regulation in DC microgrids, IEEE Trans. Smart Grid 11 (1) (2019) 577–589.

[29] L. Xing, Q. Xu, F. Guo, Z.-G. Wu, M. Liu, Distributed secondary control for DC microgrid with event-triggered signal transmissions, IEEE Trans. Sustain. Energy 12 (3) (2021) 1801–1810.

[30] Z. Chen, X. Yu, W. Xu, G. Wen, Modeling and control of islanded DC microgrid clusters with hierarchical event-triggered consensus algorithm, IEEE Trans. Circuits Syst. I. Regul. Pap. 68 (1) (2020) 376–386.

[31] S. Jena, N.P. Padhy, J.M. Guerrero, Decentralized primary and distributed secondary control for current sharing and voltage regulation in DC microgrid clusters with Hess, in: 2020 IEEE International Conference on Power Electronics, Drives and Energy Systems, PEDES, IEEE, 2020, pp. 1–7.
[32] S. Sahoo, S. Mishra, An adaptive event-triggered communication-based distributed secondary control for DC microgrids, IEEE Trans. Smart Grid 9 (6) (2017) 6674–6683.
[33] Y.-Y. Qian, A.V. Premakumar, Y. Wan, Z. Lin, Y.A. Shamash, A. Davoudi, Dynamic event-triggered distributed secondary control of DC microgrids, IEEE Trans. Power Electron. 37 (9) (2022) 10226–10238.
[34] J. Peng, B. Fan, Q. Yang, W. Liu, Distributed event-triggered control of DC microgrids, IEEE Syst. J. 15 (2) (2020) 2504–2514.
[35] Z.H.A. Al-Tameemi, T.T. Lie, R. Zamora, F. Blaabjerg, Enhanced coordination in the PV–HESS microgrids cluster: Introducing a new distributed event consensus algorithm, Energies 17 (2) (2024) 293.
[36] Z. Al-Tameemi, T. Lie, R. Zamora, F. Blaabjerg, Mixed time-state dependent distributed event-triggered consensus protocol of a DC microgrids cluster, 2024, EasyChair.
[37] Z.H.A. Al-Tameemi, T.T. Lie, R. Zamora, F. Blaabjerg, Adaptive fixed-time consensus protocol of a DC microgrids cluster, in: 2024 IEEE Power & Energy Society General Meeting, PESGM, IEEE, 2024, pp. 1–5.
[38] J. Chai, M. Wang, Z. Xu, Distributed fixed-time secondary control for DC microgrids, in: 2024 IEEE Applied Power Electronics Conference and Exposition, APEC, IEEE, 2024, pp. 1614–1618.
[39] P. Wang, R. Huang, M. Zaery, W. Wang, D. Xu, A fully distributed fixed-time secondary controller for DC microgrids, IEEE Trans. Ind. Appl. 56 (6) (2020) 6586–6597, http://dx.doi.org/10.1109/TIA.2020.3016284.
[40] S. Sahoo, S. Mishra, S.M. Fazeli, F. Li, T. Dragičević, A distributed fixed-time secondary controller for DC microgrid clusters, IEEE Trans. Energy Convers. 34 (4) (2019) 1997–2007.
[41] Q.-F. Yuan, Y.-W. Wang, X.-K. Liu, Y. Lei, Distributed fixed-time secondary control for DC microgrid via dynamic average consensus, IEEE Trans. Sustain. Energy 12 (4) (2021) 2008–2018.
[42] M. Zaery, S.M. Amrr, S.S. Hussain, M.A. Abido, Distributed event-triggered fixed-time optimal dispatch control for cyber-physical islanded DC microgrids incorporating time delays, in: 2024 IEEE Sustainable Power and Energy Conference, ISPEC, IEEE, 2024, pp. 652–657.
[43] Y.-W. Wang, Y. Zhang, X.-K. Liu, X. Chen, Distributed predefined-time optimization and control for multi-bus DC microgrid, IEEE Trans. Power Syst. 39 (4) (2024) 5769–5779.
[44] P. Hu, J.-S. Pan, S.-C. Chu, Improved binary grey wolf optimizer and its application for feature selection, Knowl.-Based Syst. 195 (2020) 105746.
[45] S. Mirjalili, S.M. Mirjalili, A. Lewis, Grey wolf optimizer, Adv. Eng. Softw. 69 (2014) 46–61.
[46] Z.-M. Gao, J. Zhao, An improved grey wolf optimization algorithm with variable weights, Comput. Intell. Neurosci. 2019 (1) (2019) 2981282.
[47] N. Yan, G. Ma, T. Yan, S. Ma, H. Zhao, Research on the double-layer intra-day management and control method of ring structure microgrid cluster based on multi-time scale, Energy Rep. 7 (2021) 18–24.
[48] M. Islam, F. Yang, M. Amin, Control and optimisation of networked microgrids: A review, IET Renew. Power Gener. 15 (6) (2021) 1133–1148.
[49] J.M. Harris, Combinatorics and Graph Theory, Springer, 2008.
[50] Y. Li, P. Dong, M. Liu, G. Yang, A distributed coordination control based on finite-time consensus algorithm for a cluster of DC microgrids, IEEE Trans. Power Syst. 34 (3) (2018) 2205–2215.
[51] P. Shafiee, M. Ahmadi, S. Najafi, Y. Batmani, Q. Shafiee, Event-triggered fully-distributed secondary control of islanded DC microgrids using pre-defined event condition, in: 2021 12th Power Electronics, Drive Systems, and Technologies Conference, PEDSTC, IEEE, 2021, pp. 1–5.
[52] Q. Liu, M. Ye, J. Qin, C. Yu, Event-triggered algorithms for leader–follower consensus of networked Euler–Lagrange agents, IEEE Trans. Syst. Man, Cybern.: Syst. 49 (7) (2017) 1435–1447.
[53] Z.H.A. Al-Tameemi, T.T. Lie, G. Foo, F. Blaabjerg, Optimal coordinated control strategy of clustered DC microgrids under load-generation uncertainties based on GWO, Electronics 11 (8) (2022) 1244.
[54] F.G. Martins, Tuning PID controllers using the ITAE criterion, Int. J. Eng. Educ. 21 (5) (2005) 867.
[55] G. Ensermu, A. Bhattacharya, N. Panigrahy, Real-time simulation of smart DC microgrid with decentralized control system under source disturbances, Arab. J. Sci. Eng. 44 (2019) 7173–7185.